Tracking Brain Development from Neonates to the Elderly by Hemoglobin Phase Measurement using Functional Near-infrared Spectroscopy

Zhenhu Liang, Hao Tian, Ho-ching (Shawn) Yang, Takeshi Arimitsu, Takao Takahashi, Angelo Sassaroli, Sergio Fantini, Haijing Niu, Yasuyo Minagawa, and Yunjie Tong

Abstract—The biological and neurological processes during the lifespan are dynamic with significant alterations associated with different stages of life. The phase and coupling of oxy-hemoglobin (Δ[HbO]) and deoxy-hemoglobin concentration changes (Δ[Hb]) measured by functional near-infrared spectroscopy (fNIRS) are shown to characterize the neurovascular and metabolic development of infants. However, the changes in phase and coupling across the human lifespan remain mostly unknown. Here, fNIRS measurements of Δ[HbO] and Δ[Hb] conducted at two sites on different age populations (from newborns to elderly) were combined. Firstly, we assessed the influence of random noise on the calculation of the phase difference and phase-locking index (PLI) in fNIRS measurement. The results showed that the phase difference is close to π as the noise intensity approaches -8 dB, and the coupling strength (i.e., PLI) presents a u-shape curve as the noise increase. Secondly, phase difference and PLI in the frequency range 0.01-0.10 Hz were calculated after denoising. It showed that the phase difference increases from newborns to 3-4-month-olds babies. This phase difference persists throughout adulthood until finally being disrupted in the old age. The children's PLI is the highest, followed by that of adults. These two groups' PLI are significantly higher than those of infants and the elderly (p<0.001). Lastly, a hemodynamic model was used to explain the observations and found close associations with cerebral autoregulation and speed of blood flow. These results demonstrate that the phase-related parameters measured by fNIRS can be used to study the brain and assess brain health throughout the lifespan.

Index Terms—Brain development; fNIRS; Phase-locking index; Hemodynamic model

I. INTRODUCTION

Human brain functions, structures, and physiologies have been studied in different age groups, including infants, young children, adults, and elderly adults. However, studying brain changes across a lifespan and identifying effective biomarkers that reflect its trajectory remains challenging [1].

Brain development throughout the lifespan is a series of complex processes. These processes include (1) physiological changes, such as the changes in blood volume/flow/speed and oxygenation [2]; (2) neural alteration, such as the changes in synaptogenesis in the cortex, the dendritic connections, and the white-matter connectivity [3]; and (3) brain functional network changes, such as changes in cortex connections [4], brain networks [5], and functional complexities [6]. Many brain imaging tools, such as electroencephalography (EEG), functional near-infrared spectroscopy (fNIRS), functional magnetic resonance imaging (fMRI), and magnetoencephalography (MEG), have been employed to investigate brain development. Among them, fNIRS, as a functional neuroimaging tool for neuroscience, has received increasing attention in recent years. The merits of fNIRS include its (1) high adaptability, (2) non-invasiveness (3) low cost, and (4) ease of integration with other imaging tools (e.g. fMRI, EEG). This makes it an irreplaceable tool in the field of neuroscience [1, 7, 8]. In addition, since the fNIRS has less restrictions on subjects and high motion-tolerance, it is an ideal imaging tool for studying infants, children, and the elderly in daily settings [9, 10].

It has been suggested that the phase of oxygenation and deoxygenation (hPod), which is the phase difference between oxy-hemoglobin (Δ[HbO]) and deoxy-hemoglobin concentration changes (Δ[Hb]), is the key to understand the hemodynamic mechanisms and brain function [11]. For early brain development, research has shown that hPod in low frequency (<0.1 Hz), is correlated with post-natal age (PNA) [12, 13]. For example, Taga et al. [7] have used the hPod and its phase-locking index (hPodL) to spatially evaluate brain development in infants. These studies and previous ones [14] all suggest that the phase difference between Δ[HbO] and Δ[Hb] is an important parameter for reflecting early brain development. Little work has been done thus far to understand these phase relationships in other age groups and how they change throughout the lifespan.

Our work is meant to fill this gap by studying the phase

Z Liang and H Tian are with the Department of Electrical Engineering, Yanshan University, Qinhuangdao, Hebei 066004, China and (e-mail: zhl@ysu.edu.cn; 1063544426@qq.com).

H Yang and Y Tong are with the Weldon School of Biomedical Engineering, Purdue University, West Lafayette, IN, USA (e-mai: yang1399@purdue.edu; tong61@purdue.edu).

T Arimitsu and T Takahashi are with the Department of Pediatrics, Keio University School of Medicine, Tokyo, Japan (e-mail: arimitsu@z8.keio.jp; ttakahashi@keio.jp).

A Sassaroli and S Fantini are with the Department of Biomedical Engineering, Tufts University, Medford, MA 02155, USA (e-mail: Angelo.Sassaroli@tufts.edu; sergio.fantini@tufts.edu).

H Niu is with the Key Laboratory of Cognitive Neuroscience and Learning, Beijing Normal University, Beijing, 100875 China (e-mail: niuhjing@bnu.edu.cn).

Y Minagawa is with the Department of Psychology, Faculty of Letters, Keio University, Tokyo, Japan (e-mail: myasuyo@bea.hi-ho.ne.jp).

Dr. Yunjie Tong is the author to whom correspondence should be addressed.

difference between $\Delta[Hb]$ and $\Delta[HbO]$ (i.e. $Arg(\Delta[Hb])-Arg(\Delta[HbO])$) in different cohorts of human subjects from neonates to the elderlies. Moreover, the phase-locking index (PLI), which has been suggested to be correlated with the developmental stages of metabolism, blood flow, circulatory, and neurovascular functions [7, 12], was used to investigate the coupling changes between $\Delta[HbO]$ and $\Delta[Hb]$ in different age groups.
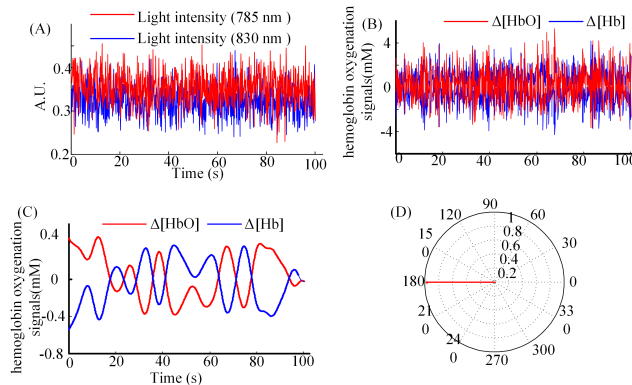

Fig. 1. The phase difference and coupling strength calculation are based on two noise light intensity signals. (a) Two light intensity waves of 785 nm and 830 nm were recorded from the fNIRS system. (b) The $\Delta[Hb]$ and $\Delta[HbO]$ signals were calculated from the light intensity signals based on the modified Beer–Lambert law. (c) Filtered $\Delta[Hb]$ and $\Delta[HbO]$ signals in the 0.01-0.1 Hz frequency band. (d) Phase difference between $Arg(\Delta[Hb])-Arg(\Delta[HbO])$ and PLI for the two signals in (c).

It is well-known that phase difference is an important biomarker to analyze the hemodynamic characteristics of the brain [15, 16]. However, we observed an interesting phenomenon that the $\Delta[HbO]$ and $\Delta[Hb]$ derived from the pure-noise channel (with the standard preprocess procedure) were anti-phased with each other, as shown in Fig. 1. The systematic result derived from seemly random noise is alarming. We conducted several simulations to understand the impact of noise on the phase calculations.

Lastly, the dynamic model proposed by Fantini [2] was used to identify the key vascular/physiological parameters that cause changes in the phase difference. Even though the model includes eight parameters that affect the phase relationship [17], the most relevant parameters for this study are (1) the capillary transit time ($t^{(c)}$), (2) the venous transit time ($t^{(v)}$), and (3) the dynamic autoregulation cut-off frequency (Hz).

II. MATERIALS AND METHODS

A. Participants

This study included 161 healthy participants involving infants, young children, adults, and elderly adults, and it covered the ages of a large portion of the human lifespan. The data collection was taken place at two different sites.

1) Infants from Keio University

Japanese infant data was collected from Keio University, Tokyo, Japan. It consisted of data from 21 preterm infants (11 boys and 10 girls, gestational age (GA) > 34 weeks), 20 term infants (12 boys and 8 girls, GA ≥ 37 weeks) and 27 3-4-month-olds infants (10 boys and 17 girls, GA ≥ 37 weeks) in sleeping status. Apgar score was employed to evaluate the health state of early preterm and term infants. The Apgar scores

of early preterm and term infants at 5 minutes after birth are 7.60 ± 1.19 and 8.02 ± 1.56, respectively, suggesting fair birth condition for the preterm and good condition for the term neonates [18]. The Enjoji's developmental test applied to the 3-4-month-olds revealed that their developmental quotient including motor, social and language abilities are within the normal range. Details for all subjects are presented in Table I. The subjects' parents signed the informed consent from the Keio University Hospital ethics committee before the measurements (No. 20090189). All neonates and infants were measured in a dimly lit room while sleeping. The sleeping status was judged by their frequent motor activity and rapid eye movements.

TABLE I
DEMOGRAPHIC CHARACTERISTICS OF THE INFANTS

characteristics	Early preterm	Term	3-4 months
total(boy/girl)	21(11/10)	20(12/8)	27(10/17)
PMA(wk)	37.9(34-45.1)	39.0(37.4-41.5)	57.1(51.8-61.7)
GA(mean(min-max))(wk)	30.1(23-33.4)	38.4(37-41)	39.5(37.4-41.5)
PNA(day)	54.6(17-137)	4.2(3-7)	122.8(97-146)
Birth weight (mean(min-max)) (g)	1282.7(463-1887)	2851.8(2300-3936)	2937.5(2420-3562)
Characteristics	Children	Adults	Healthy elderlies
Total(male/female)	21(10/11)	20(12/8)	27(15/12)
Age(mean(min-max)) (years)	8.1(6-11)	23.2(19-27)	63.3(58-77)
BMI(mean(min-max))	17.2(16-19)	21.3(19-24)	20.9(18.5-23)

The ETG-4000 NIRS system (Hitachi Medical Corporation) measured the relative fluctuations in $\Delta[HbO]$ and $\Delta[Hb]$ (millimolar(mM)). The fNIRS probes used on the early preterm and term neonates were different from those of 3-4-month-olds infants. The fNIRS probe used on neonates included 46 source-detector channels. The layouts of the probes on a standard brain model are shown in Figs. 2 (a)-(c), where the crosses and the empty circles are the positions of the light sources and the detectors to identify the channels. The source and detector mounted on the left and right temporal regions were set of two 12 channels arrays (3 sources and 3 detectors), the frontal region was set of one 22 channels array (3 sources and 5 detectors). The fNIRS probe used on the 3-4-month-olds infants includes 44 source-detector channels. The layouts in different views are shown in Figs. 2 (e)-(g). Two sets of 22 channels with 3 sources and 5 detectors arrays were used to mount the frontal, left, and right temporal regions. The corresponding locations of the 46 and 44 fNIRS channels are shown in Figs. 2(d) and (h), respectively. The positions of the probe arrays are selected according to the international 10-20 system [19].

The anatomical areas covered by fNIRS were divided into 3 regions for spatial investigation: frontal cortex, left temporal cortex, and right temporal cortex. The distance between the source and detector was approximately 2 cm. The fNIRS sampling rate was 10 Hz and the wavelengths of the near-infrared lights were 695 nm and 830 nm, respectively. We used the NIRS-SPM toolbox to convert the light intensity into $\Delta[Hb]$ and $\Delta[HbO]$ by using the modified Beer-Lambert Law [20]. The differential path-length factor (DPF) was set as 6.1718 and 5.5374 for the two wavelengths.

2) Children, adults, and the elderly from Beijing Normal University

The fNIRS data from children to elderly adults were collected from Beijing Normal University, Beijing, China. The study enrolled 68 normal healthy participants-21 children (aged 6-11, 10 males, 11 females), 20 adults (aged 19-27, 12 males, 8 females), and 27 healthy elderly adults (58-77, 15 males, 12 females). All subjects were right-handed Han Chinese with normal or corrected-to-normal vision. The detailed information of the children and adults were described in the study of [21], while the healthy elderlies were presented in the study of [22]. All these participants were considered healthy with normal weight. The body mass index (BMI) with the ranges of 16-19 for children and 18.5-24 for adults (including elderlies) were used as enrollment criteria. An informed consent form was signed before the experiments by either the subjects or their parents (for minors). The experiments were approved by the Institutional Review Board of Beijing Normal University, China. The participants with the following symptoms were excluded for analysis: (1) depression (Hamilton depression rating scale $\geq$ 24 points); (2) histories of stroke, nervous system diseases, and other systemic diseases that can cause cognitive impairment; (3) histories of psychosis or congenital mental growth retardation. The neuropsychological tests used for the healthy elderlies are the Chinese version of mini-mental state examination (MMSE), the Beijing version of Montreal cognitive assessment (MoCA), clinical dementia rating (CDR), and so on [22]. Lastly, additional enrollment criteria for healthy elderlies were employed. They are: (1) no complaint of memory or other cognitive impairment, (2) CDR score is 0, and (3) no severe visual or auditory impairment.

The recording process has been described in detail by Cai et al. [14]. A continuous wave near-infrared optical imaging system (CW6, TechEn Inc., MA, U.S.A) recorded the hemodynamic response in a resting state. Twelve transmitters and 24 receivers (forming 46 measurement channels) with a source-detector distance of 3.2 cm were placed on a stretchable cap covering most of the head. The layouts are shown in Figs. 2(i)-(k). The corresponding locations of 46 channels as reference to the international 10-20 system are shown in Fig. 2(l) and they covered the frontal, parietal, temporal, and occipital cortices regions. The wavelengths of the light are 690 nm and 830 nm, respectively. The sampling rate of the system is 50 Hz and the duration of the experiment was approximately 11 minutes, while the subject was in a relaxed, eyes closed, but awake state.

We used the Homer2 to convert the light intensity into Δ[Hb] and Δ[HbO] by using the modified Beer-Lambert Law [15]. The extinction factors proposed by Gratzer [23, 24] were used for the calculation and the DPF was set as 6.0 in all these participants. More details about the DPF could be found in Refs [25, 26]. Because we analyzed the phase difference and coupling of Δ[Hb] and Δ[HbO] rather than the hemodynamic oscillation itself, the DPF and extinction factor used have little effect on the results [5].
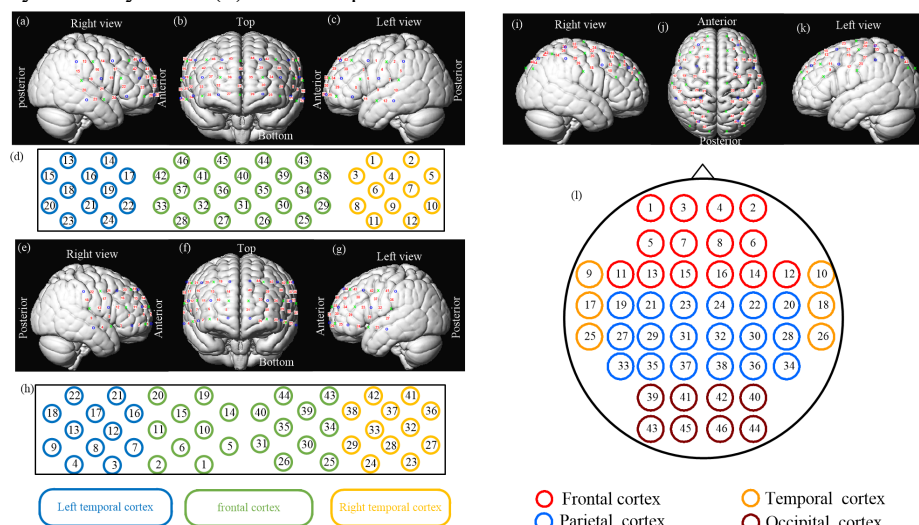

Fig. 2. Schematic arrangement of fNIRS channels for neonates (preterm and term infants), children, adults, healthy elderlies. (a)-(c) Three views (left, front, and right) of fNIRS probe arrays over a brain model with 46 channels for neonates (preterm and term infants). (d) Anatomical areas covered by 46 fNIRS channels. The colors represent the different cortical regions. (e)-(g) Three views of 44 channel fNIRS probe arrays for 3-4-month-olds infants. (h) Anatomical areas covered by 44 fNIRS channels similar to those in (d). (i)-(k) Three views (right, top, and left) of fNIRS probe arrays over a brain model with 46 channels for children, adults, and the healthy elderly. The electrodes cover the frontal, temporal, parietal, and occipital regions. (l) Spatial position of each measurement channel.

B. Data Preprocessing

This study calculated the log-power of the Δ[HbO] with the multitaper spectral method in the Chronux toolbox (version 2.11; hppt://chronux.org/. Accessed July 15, 2018). Signal quality is critical in analyzing the phase of hemodynamic oscillations. Therefore, the following two quality control steps were conducted: 1) The NIRS channel without the cardiac component (~1Hz) in the spectrum was regarded as the noise signal and was removed from further analysis. We excluded the participant with over 20% bad channels (i.e., without the cardiac signal or only with random noise) from further analysis (only 2 participants were excluded due to this reason). For the remaining participants, if the proportion of the bad channels is less than 20% (5 participants were in this situation), the bad channels were excluded from further statistical analysis. 2) The kurtosis-based Wavelet Filtering (kbWF) was used to correct motion artifact [27]. Based on the previous study [27], we set the kurtosis threshold

as 3.3, a Daubechies 5 (db5) wavelet for the discrete wavelet transformation, and decomposition level as 10, in the data preprocessing. The detailed motion-correction processes were shown in Fig. S1 (supplement Part I).

After motion correction, all data were resampled to 2 Hz before the low-frequency hemodynamic components (i.e. (1) 0.01-0.05 Hz; (2) 0.05-0.1 Hz and (3) 0.01-0.1 Hz). We adopted 2 Hz for redundancy [28] and to be consistent with our previous study [13]. The low-frequency signals were extracted with a zero-phase digital band-pass filter (Matlab function of filtfilt.m, butterworth order=3).

C. Time-varying Arg(Δ[Hb])-Arg(Δ[HbO]) and PLI

After band-pass filtering, the time-varying Arg(Δ[Hb])-Arg(Δ[HbO]) and PLI were calculated to measure the phase difference and coupling of Δ[HbO] and Δ[Hb]. We note that this phase difference (Δ[Hb] relative to Δ[HbO]) is the opposite of the one that defines hPod (Δ[HbO] relative to Δ[Hb]). Also, the hPod measurement regarded the testing state as a static, not a dynamically fluctuating state. In this study, a fixed epoch length of 120 s and 90% overlap was used to derive the variation of phase difference over time to characterize the dynamic hemodynamic processes. The detailed calculation processes are described below for each range of the low-frequency hemodynamic oscillations.

(1) The Δ[HbO] and Δ[Hb] recordings from one channel were divided into n windows with the overlap of 90%, where the window length was 120 seconds, For a recording length of l, the number n equal to $round\left(\dfrac{l - WL * fs}{(1 - overlap) * WL * fs}\right) + 1$, where the WL and $overlap$ values are 120 and 0.9, respectively.

(2) The Δ[HbO] and Δ[Hb] segments were referred to as $x(t)$ and $y(t)$, respectively. Based on the Hilbert transform, the signals' instantaneous phases (IP) were:

$$\varphi_x(t) = \tan^{-1}\frac{Im(x_a(t))}{Re(x_a(t))} \text{ and } \varphi_y(t) = \tan^{-1}\frac{Im(y_a(t))}{Re(y_a(t))} \quad (1)$$

where $x_a(t)$ and $y_a(t)$ were the analytic signal representation of $x(t)$ and $y(t)$, respectively.

(3) Then, the phase difference between φ_x and φ_y ($\Delta\varphi_{xy} = \varphi_x - \varphi_y$) was calculated and projected in $[0, 2\pi]$.

(4) The *PLI* measurement was defined as:

$$PLI(t) = \frac{1}{N}\left|\sum_{t=1}^{N} e^{j\Delta\phi_{xy}(t)}\right| \quad (2)$$

where N was the length of $x(t)$ and $y(t)$. The *PLI* was bounded between 0 and 1.

Lastly, for one channel we can get n phase difference and *PLI* values. The number of n based on the testing duration time. To get a consistent statistical comparison between different age groups, we selected the samples with a testing time of more than 3 minutes for statistics.

D. Statistical analysis

This study investigated the phase difference and coupling characteristics of hemodynamics with brain development and aging. We used the violin plot and box plot to show the distribution of the samples at channel-based and region-based statistical analysis, respectively. Given that the phase difference indices are angle values, a circular statistics toolbox was used for statistical analysis [29]. The parametric Watson-Williams multi-sample test was used to determine significant differences of Arg(Δ[Hb])-Arg(Δ[HbO] between groups [13]. For the PLI, a Lilliefors test determined whether the values had a normal distribution. The Kruskal-Wallis test and multiple comparison tests with Bonferroni correction were performed to determine significant differences between the indices of different age groups. A two-way repeated analysis of variance (two-way ANOVA) was applied to assess the interactions and the main effects on the two dependent variables (Arg(Δ[Hb])-Arg(Δ[HbO], and PLI) for the two conditions: age group and brain region. After obtaining the interactions and the main effects on the two dependent variables, a post-hoc test with Bonferroni correction determined the significant difference of the phase difference (Arg(Δ[Hb])-Arg(Δ[HbO])) and PLI indices among various brain regions (i.e., frontal, left temporal, and right temporal regions) in each age group (i.e., preterm infants, term infants, 3-4-month-olds infants, children, adults, and healthy elderly). Adjusted p-values below 0.05 were considered to indicate statistically significant difference. The same statistical tests were performed at the channel-based level and region-based level, respectively. In the Figs and tables, p<0.05, p<0.01, and p<0.001 are marked with '*', '**', and '***', respectively.

E. Impact of random noise on phase calculation

In order to analyze the noise effect on the anti-phase trend of Δ[Hb] and Δ[HbO] based on the modified Beer-Lambert law in more detail, we considered two scenarios.

For the first one, the random noise of varying intensities was added to the raw optical density signals. We selected the raw optical density signals that had distinct heart rate information and assumed those signals are relatively "clean" signals. For the noise channel, we set the source and detector in a dark environment away from the subject. So that we can get a pure noise signal that doesn't contain hemoglobin signals. We added the noise to the raw optical density signals with the noise coefficient from 0 to 1. To obtain the phase difference changes at different noise levels, we set the step to 0.01 in the range of 0 to 0.1 and 0.1 in the range from 0.05 to 1. Finally, the signal-to-noise ratio (SNR) of the signal in different levels of noise was calculated by dividing the energy of raw optical density by noise energy.

For the second scenario, we employed a mathematical model to simulate the real optical density signals, which can ensure that there is no noise in the signals. Two sinusoidal signals with a low frequency of 0.01 Hz modulated by a frequency of 1 Hz under a sampling rate of 10 Hz numerically simulated the noise effect on the phase calculation. The formulas are described as follows:

$$\begin{cases} x = 2\sin(2\pi t) + 2\sin(2\pi * 0.1t) + 8\sin(2\pi * 0.01t) + 50 \\ y = \sin(2\pi t) + \sin(2\pi * 0.1t) + 4\sin(2\pi * 0.01t) + 20 \end{cases} \quad (3)$$

Gaussian random noise was generated by the MATLAB function *randn.m* and added to the signals (x and y). The noises' amplitudes that added to the two sinusoidal signals were set as 8 and 4, respectively. Similar to the scenario 1, the

coefficient of noise adds in signal x and y from 0 to 0.1 at steps of 0.01 and from 0.1 to 1 at steps of 0.05. Different levels of the SNR were calculated dividing the signal energy by the noise energy.

III. HEMODYNAMIC MODEL

This study employed a recent hemodynamic model [30] to explain the phase difference between $\Delta[Hb]$ and $\Delta[HbO]$ that are associated with brain development and aging. This may shed light on the underlying physiological changes. This model is a dynamic extension of the steady-state hemodynamic model previously proposed by Fantini [31]. Using the previous model, Watanabe et al. [12] found that the partial blood volume contributes to the in-phase, whereas, the partial pressure of oxygen, oxygen utilization rate, and the speed of blood flow contributes to the anti-phase of $\Delta[HbO]$ and $\Delta[Hb]$, respectively. The phasors that describe the oscillations of $\Delta[Hb]$ and $\Delta[HbO]$ are termed $\mathbf{O}(\omega)$ and $\mathbf{D}(\omega)$, respectively, and are related to $cbv(\omega)$, $cbf(\omega)$ and $cmro_2(\omega)$ (the phasors representing the oscillations of cerebral blood volume (CBV), cerebral blood flow (CBF), and cerebral metabolic rate of oxygen (CMRO2), respectively), according to the following equations:

$$\mathbf{O}(\omega) = ctHb\left[S^{(a)}CBV_O^{(a)}\mathbf{cbv}^{(a)}(\omega) + S^{(v)}CBV_0^{(v)}\mathbf{cbv}^{(v)}(\omega) \right] +$$
$$ctHb\left[\frac{<S^{(c)}>}{S^{(v)}}(<S^{(c)}> - S^{(v)})\mathbf{F}^{(c)}CBV_0^{(c)}H_{RC-LP}^{(c)}(\omega) + \right. \tag{4}$$
$$\left. (S^{(a)} - S^{(v)})CBV_0^{(v)}H_{G-LP}^{(v)}(\omega) \right]\left[\mathbf{cbf}(\omega) - \mathbf{cmro}_2(\omega)\right]$$

$$\mathbf{D}(\omega) = ctHb\left[(1-S^{(a)})CBV_0^{(a)}\mathbf{cbv}^{(a)}(\omega) + (1-S^{(v)})CBV_0^{(v)}\mathbf{cbv}^{(v)}(\omega) \right] +$$
$$ctHb\left[\frac{<S^{(c)}>}{S^{(v)}}(<S^{(c)}> - S^{(v)})\mathbf{F}^{(c)}CBV_0^{(c)}H_{RC-LP}^{(c)}(\omega) + \right. \tag{5}$$
$$\left. (S^{(a)} - S^{(v)})CBV_0^{(v)}H_{G-LP}^{(v)}(\omega) \right]\left[\mathbf{cbf}(\omega) - \mathbf{cmro}_2(\omega)\right]$$

We define also the ratio of $\Delta[Hb]$ and $\Delta[HbO]$ phasors as:

$$\frac{\mathbf{D}(\omega)}{\mathbf{O}(\omega)} = \frac{|\mathbf{D}(\omega)|}{|\mathbf{O}(\omega)|}e^{i\{Arg[\mathbf{D}(\omega)] - Arg[\mathbf{O}(\omega)]\}} \tag{6}$$

In Eq.(4) the superscripts "(a)", "(v)" and "(c)" indicate the contributions from arterial, venous, and capillary compartments, respectively, for oxygen saturation ($S^{(a)}$, $S^{(v)}$, and $<S^{(c)}>$), baseline cerebral blood volume ($CBV_0^{(a)}$, $CBV_0^{(v)}$, $CBV_0^{(c)}$) in units of ml_{blood}/g_{tissue}, and oscillations of cerebral blood volume ($\mathbf{cbv}^{(a)}$, $\mathbf{cbv}^{(v)}$) We note that with lower case characters we indicate unitless phasors (that describe oscillations normalized to a baseline value). On the contrary, HbO and Hb phasors express absolute changes (not normalized) and are expressed in units of micromolar. Finally, $H_{RC-LP}^{(c)}(\omega)$ and $H_{G-LP}^{(v)}(\omega)$ are the capillary and venous complex transfer functions (which depend on the capillary and venous transit times), $\mathbf{F}^{(c)}$ indicates the Fahraeus factor, the ratio of capillary-to-large vessel hematocrit, and $ctHb$ is the concentration of total hemoglobin in blood [17, 30].

We used the hemodynamic model to calculate the phase difference $Arg(\Delta[Hb])-Arg(\Delta[HbO])$ with various values of capillaries ($t^{(c)}$), and veins ($t^{(v)}$) transit times, and autoregulation cutoff frequency[2, 17, 30]. We note that the

model predicts negative values for $Arg(\Delta[Hb])-Arg(\Delta[HbO])$ (i.e. oscillations of Hb that are lagging oscillations of oxyhemoglobin). However, phase angles are defined to within a multiple of 2π, and the experimental results reported here are projected in the interval $[0, 2\pi]$. The relevant findings of changes in the relative phase of $\Delta[Hb]$ vs. $\Delta[HbO]$, specifically an increase with age, are independent of the choice for the phase sign: it corresponds to more positive phase values (in the representation of experimental results) or less negative phase values (in the representation of the hemodynamic model).

IV. RESULTS

A. The effects of the anti-phase trend of Δ[Hb] and Δ[HbO] based on the calculation of the modified Beer–Lambert law with the influence of noise

Firstly, we analyzed the underlying effect of modified Beer-Lambert law to the anti-phase trend of $\Delta[Hb]$ and $\Delta[HbO]$. The concentration changes of $\Delta[Hb]$ and $\Delta[HbO]$ are commonly obtained from the following equation:

$$\Delta[Hb] = \frac{\varepsilon_{HbO}^{\lambda_2}\dfrac{\Delta OD^{\lambda_1}}{B^{\lambda_1}} - \varepsilon_{HbO}^{\lambda_1}\dfrac{\Delta OD^{\lambda_2}}{B^{\lambda_2}}}{\left(\varepsilon_{Hb}^{\lambda_1}\varepsilon_{HbO}^{\lambda_2} - \varepsilon_{Hb}^{\lambda_2}\varepsilon_{HbO}^{\lambda_1}\right)L} \tag{7}$$

$$\Delta[HbO] = \frac{\varepsilon_{Hb}^{\lambda_1}\dfrac{\Delta OD^{\lambda_2}}{B^{\lambda_2}} - \varepsilon_{Hb}^{\lambda_2}\dfrac{\Delta OD^{\lambda_1}}{B^{\lambda_1}}}{\left(\varepsilon_{Hb}^{\lambda_1}\varepsilon_{HbO}^{\lambda_2} - \varepsilon_{Hb}^{\lambda_2}\varepsilon_{HbO}^{\lambda_1}\right)L} \tag{8}$$

Where $\varepsilon_{Hb}^{\lambda}$ is the extinct coefficient of Hb at wavelength λ; $\varepsilon_{HbO}^{\lambda}$ is the extinct coefficient of HbO at wavelength λ; we employed the extinction factor proposed by Gratzer [23, 24] for converting the light intensity into $\Delta[Hb]$ and $\Delta[HbO]$ by using the modified Beer-Lambert Law [20]. ΔOD^{λ} is the change in optical density at the wavelength λ (from the baseline), B^{λ} is the DPF at wavelength λ, and L is the distance between source and detector.

From equations 7 and 8, we can see that $\Delta[HbO]$ is associate with $\dfrac{\varepsilon_{HbO}^{\lambda_2}}{B^{\lambda_1}}\Delta OD^{\lambda_1} - \dfrac{\varepsilon_{HbO}^{\lambda_1}}{B^{\lambda_2}}\Delta OD^{\lambda_2}$, while $\Delta[Hb]$ is associated with $\dfrac{\varepsilon_{Hb}^{\lambda_1}}{B^{\lambda_2}}\Delta OD^{\lambda_2} - \dfrac{\varepsilon_{Hb}^{\lambda_2}}{B^{\lambda_1}}\Delta OD^{\lambda_1}$ (i.e., ΔOD^{λ_s} have changed the signs). If ΔOD^{λ_1} and ΔOD^{λ_2} are random noise, the averaged phase of $\Delta[HbO]$ and $\Delta[Hb]$ is tended to be π (or $-\pi$), as demonstrated in Fig. 1.

We analyzed the influence of the random noise on the phase difference and PLI under two different scenarios. The detailed processes and results were shown in the supplement Part II. The simulations showed that the random noise is not a negligible factor for the phase difference and PLI calculation.

Also, the impact of the device difference was considered in this study. The detailed contents were presented in the supplement Part III.

B. Changes in phase difference with brain development

Fig. 3 shows examples of two types of $\Delta[HbO]$ vs. $\Delta[Hb]$ oscillations patterns. In Fig. 3(a), the hemodynamic oscillations

of Δ[HbO] and Δ[Hb] are derived from an adult subject. The data length of this epoch is 100 s with a 0.01-0.1 Hz frequency band. The phase difference between Δ[HbO] and Δ[Hb] is π (see Fig. 3(b)). Fig. 3(c) presents another oscillation pattern, derived from one preterm neonate with a time length of 100s in the same frequency band. As shown, the phase difference is approximately $\pi/2$ for this subject (see Fig. 3(d)).
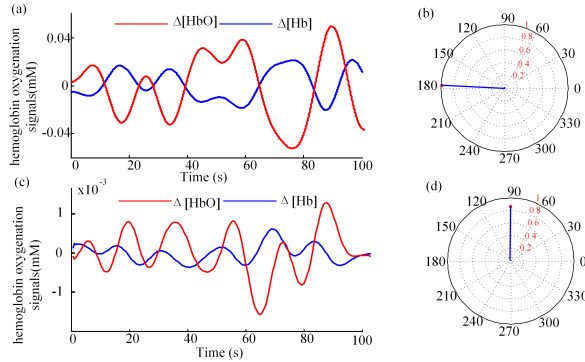

Fig. 3. Δ[HbO] and Δ[Hb] oscillations. (a) Δ[HbO] and Δ[Hb] signals (0.01-0.1 Hz) recorded from the adults. (b) Vector representation of Arg(Δ[Hb])-Arg(Δ[HbO]) and PLI (length of vector) for the signals in (a). (c) Δ[HbO]and Δ[Hb] signals (0.01-0.1 Hz) recorded from the preterm. (d) Vector representation of Arg(Δ[Hb])-Arg(Δ[HbO]) and PLI for the signals in (c).

To investigate changes in the phase difference with brain development and aging, the time-varying phase differences (i.e., Arg(Δ[Hb])-Arg(Δ[HbO])) were calculated for each age group (early preterm, term, 3-4-month-olds infants, children, adults, and the elderly) in every channel. The post-natal age (PNA) for early preterm and term was 54.6 (17-137) days and 4.2(3-7) days, respectively. The variation ranges of the phase differences in six individual subjects from different age groups were calculated and showed in Fig. 4. The variation ranges (red sector) for the early preterm and term are close to $\pi/2$ (see in Fig. 4(a) and 4(b)). While the phase difference ranges in most channels in 3-4-month-olds infants are close to π (Fig. 4(c)). Similar phenomena can also be found in the children (6 years) and adults (27 years) (see Fig. 4(d) and 4(e)). It is interesting that the phase difference variations in the healthy elderly (Fig. 4(f) have a wider range than other subjects (Fig. 4(f)). The mean phase differences (blue line in the red sector) in some channels are close to $\pi/2$.

The distribution of the time-varying phase differences with all the channels (more than 5 segments in one channel' recording) in each age group (in 0.01-0.05 Hz) is shown in Fig. 5. As shown, the most phase difference between the early preterm and term was within the range of $[\pi/2,\pi]$. Whereas, the values in the 3-4-month-olds infants, children, and adult groups were around π (evenly distributed around π). Among the healthy elderly, the values were broadly distributed within the range of $[0,\pi]$, indicating greater variability. In addition, the phase difference indices for these groups in 0.05-0.1 Hz and 0.01-0.1 Hz are shown in Figs. S5 and S6 (see in Supplement Part IV (1)) with similar observations.

The mean and SD of the phase difference and PLI for all age groups in the 0.01-0.05 Hz, 0.05-0.1 Hz, and 0.01-0.1 Hz frequency bands are present in Tables II and III, respectively. As shown, the Arg(Δ[Hb]) leads the Arg(Δ[HbO]) by

approximately 1.78 and 1.32 rad (mean), in the 0.05-0.1 Hz frequency band for early preterm and term infants, respectively. Of course, a lead by x radians is equivalent to a lag by 2π $-x$ radians, and we observe again that it was argued that Δ[Hb] should be interpreted as lagging Δ[HbO]. The term infants (with a PNA of 4.2 days (mean value)) had significant in-phase tendency compared with those of the early preterm (with a PNA of 54.6 days) and 3-4-month-olds infants (with PNA of 122.8 days (mean value)) in the 0.05-0.1 Hz, 0.05-0.1 Hz, and 0.01-0.1 Hz frequency bands. This finding indicated that the phase difference was mainly correlated with PNA age (i.e., at the time of the measurement) in the infant groups, regardless of the infants' status (preterm or term). Lastly, the variations of the phase difference in healthy elderlies are larger than those of adults.

TABLE II
THE STATISTICS OF ARG(Δ[HB])-ARG(Δ[HBO]) WITH DIFFERENT AGE GROUPS (EARLY PRETERM, TERM, 3-4 MONTHS, CHILDREN, ADULTS, AND HEALTHY ELDERLIES) IN 0.01-0.05 HZ, 0.05-0.1 HZ AND 0.01-0.1 HZ

	0.01-0.05Hz Mean ± SD	0.05-0.1Hz Mean ± SD	0.01-0.1Hz Mean ± SD
Early preterm	2.19±0.60	1.78±0.46	2.08±0.50
Term	1.99±0.72	1.32±0.46	1.85±0.58
3-4 months	2.75±0.62	2.56±0.49	2.71±0.54
children	2.87±0.23	2.87±0.21	2.86±0.20
Adults	2.53±0.63	2.37±0.92	2.49±0.64
Healthy elderlies	2.33±0.94	2.28±1.89	2.14±1.08

TABLE III
THE STATISTICS OF PLI WITH DIFFERENT AGE GROUPS (EARLY PRETERM, TERM, 3-4 MONTHS, CHILDREN, ADULTS, AND THE HEALTHY ELDERLIES) IN 0.01-0.05 HZ, 0.05-0.1 HZ AND 0.01-0.1 HZ

	0.01-0.05Hz Mean ± SD	0.05-0.1Hz Mean ± SD	0.01-0.1Hz Mean ± SD
Early preterm	0.58±0.18	0.63±0.18	0.55±0.17
Term	0.58±0.16	0.65±0.19	0.55±0.15
3-4 months	0.60±0.19	0.62±0.20	0.57±0.19
Children	0.79±0.19	0.79±0.19	0.77±0.20
Adults	0.73±0.22	0.70±0.25	0.68±0.25
Healthy elderlies	0.53±0.14	0.56±0.17	0.48±0.15

The PLI is a parameter that measures the coupling strength of Δ[Hb] and Δ[HbO]. The results show that the children and adults have higher values than the rest of the participants, which might indicate that the coupling strengths of Δ[Hb] and Δ[HbO] slightly increase with brain development and decrease with brain aging.

The significance of the phase difference indices among different age groups is calculated with the Watson-Williams multi-sample test. The results showed that from 0.01-0.05 Hz, the phase differences are significantly different among all age groups (Table S3 in Supplement Part IV (2)). Whereas, for 0.05-0.1 Hz and 0.01-0.1 Hz, not all age groups show a significant difference from each other (Tables S4 and S5 in Supplement Part IV (2)). This means that cerebral vascular development might be frequency-dependent. Also, the Kruskal-Wallis test and multiple comparison tests were used to determine the PLI significance for different age groups. The groups of children and adults had significantly higher values than those of the infants and the elderly adults for the 0.01-0.05 Hz and 0.01-0.1 Hz frequency bands ($p<0.001$) (Tables S6-S8 in Supplement Part IV (2)). However, there were no significant differences among the infants (i.e., early preterm, term, and 3-4 months) (Tables S6-S8 in Supplement Part IV (2)). It may

indicate that, unlike phase difference, PLI might not be as sensitive in the first few months of life.

Furthermore, the spatial specificity of selected regions (i.e., frontal, left temporal, and right temporal cortices) of phase difference and PLI were calculated for all age groups. The regions were chosen due to the overlapping coverages of the fNIRS probes on all participants. The averaged phase difference values and PLIs in each channel were regarded as samples for statistics. Fig. 6 shows the spatial distribution of phase difference and PLI in the 0.01-0.05 Hz frequency band in the frontal, left temporal, and right temporal cortices. The violin plots of phase difference and PLI in the 0.05-0.1 Hz and 0.01-0.1 Hz are shown in Figs. S7 and S8 (see in Supplement Part IV (3)), respectively. The width of each 'violin' reflects the distribution of these indices in each region at every age group. The mean ± SD of the phase difference and PLI range in each cortical region for each frequency band are presented in Tables S9 and S10 (see in Supplement Part IV (3)).
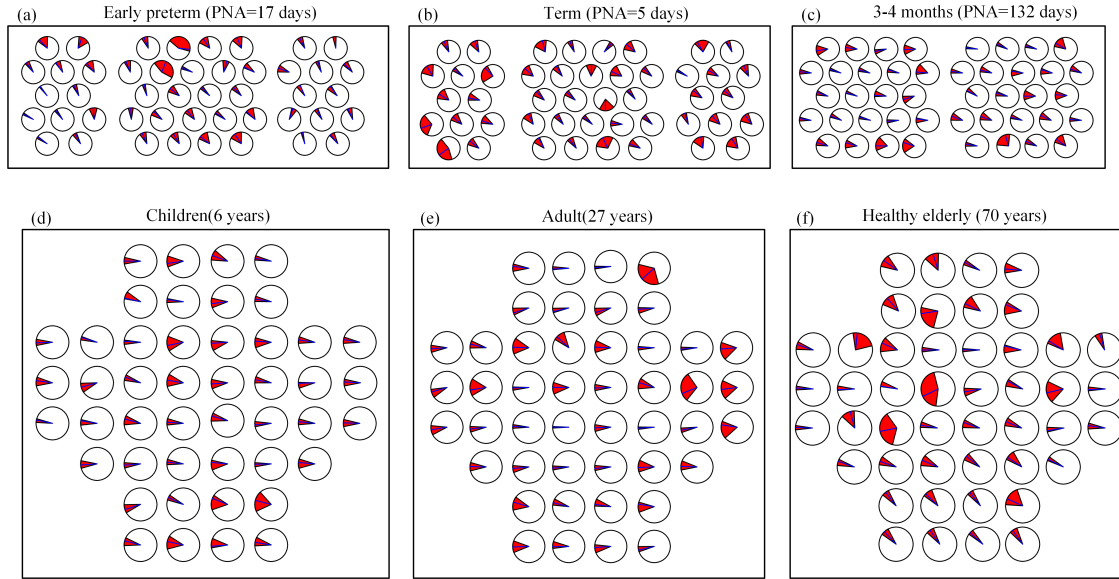

Fig. 4. The variation of time varying Arg(Δ[Hb])-Arg(Δ[HbO]) in different subjects in different age groups. (a)-(c) are the time varying phase difference in spatial scale in the subjects with the age of PNA=17, 5 and 132 days. The blue lines in the red sectors and the range of red sectors are the mean and SD values of the Arg(Δ[Hb])-Arg(Δ[HbO]) during time course in each channel. Similar as (a)-(c), the (d)-(f) are the variation of time varying Arg(Δ[Hb])-Arg(Δ[HbO]) in the subjects with the age of 6 years, 27 year, and 70 years.
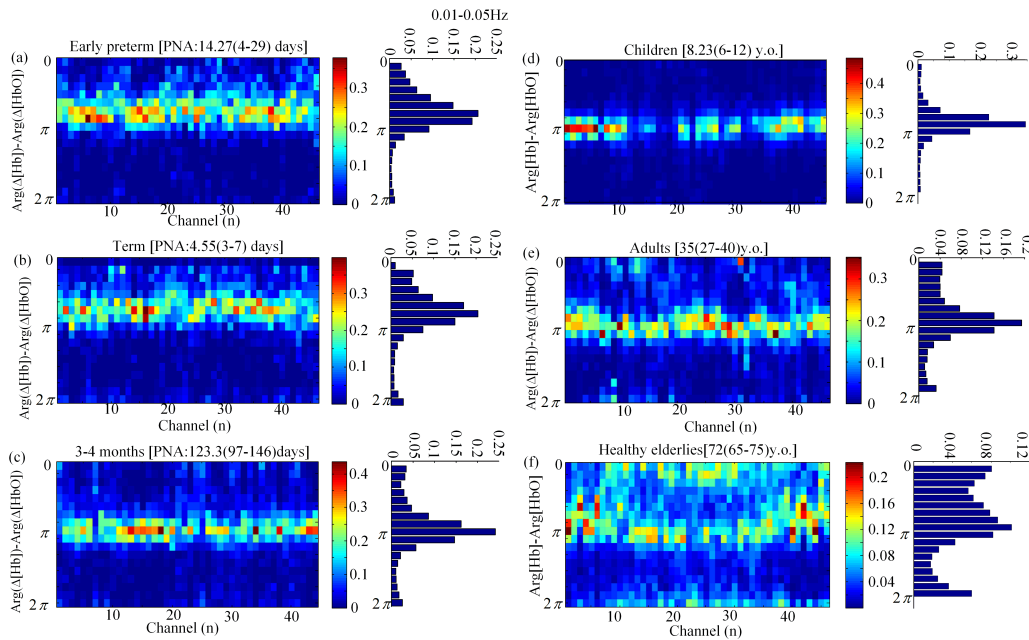

Fig. 5. Arg(Δ[Hb])-Arg(Δ[HbO]) distribution in each channel for all age groups in the 0.01-0.05 Hz frequency band. (a) Arg(Δ[Hb])-Arg(Δ[HbO]) distribution with every channel for early preterm infants (left part) and proportion of Arg(Δ[Hb])-Arg(Δ[HbO]) in each phase bin (right part). (b)-(f) similar measurement of the Arg(Hb)-Arg(HbO) for the term infants, 3-4-month-olds infants, children, adults, and elderly participants.

The sample numbers of phase differences for all ages that were employed for statistical analysis in three frequency bands are 3731, 3834, 3729, respectively. For the phase difference measure, a two-way ANOVA test showed that the

main effects with the factors conditions of age groups (n=6: preterm, term, 3-4 months, children, adults, and the healthy elderlies) and brain regions (n=3: frontal, let temporal, and right temporal cortex) were both significant for 0.05-0.1 Hz and 0.01-0.1 Hz. Also, the interactions of the two factors were significant only in 0.05-0.1 Hz (F (10, 3816) =3.490, p=0.000). All results of the two-way ANOVA tests are shown in Table S11 (see in Supplement Part IV (4)). The statistical analysis of significant differences between two of the three regions

(frontal, left temporal, and right temporal) for every age group in the 0.01-0.05 Hz, 0.05-0.1 Hz, and 0.01-0.1 Hz frequency bands are presented in Table S12(see in Supplement Part IV (4)). As shown, there were no significant differences for most age groups. For each cortical region, the significant differences are obvious among infants' groups (preterm, term, and 3-4 months), but not for the age groups from children to healthy elderly (Tables S13-S15 in Supplement Part IV (4)). The significant difference is also frequency-dependent.
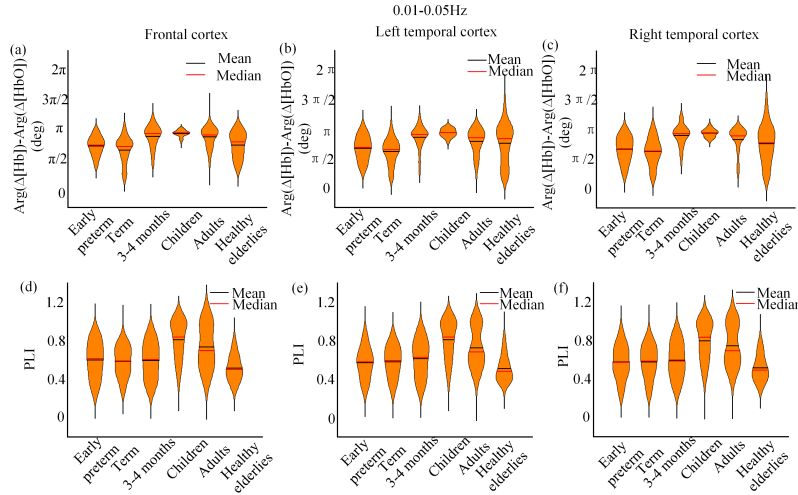

Fig. 6. Violin plots of the Arg(Δ[Hb])-Arg(Δ[HbO]) and PLI for different age groups in different spatial areas. (a)-(c) Violin plots of the Arg(Δ[Hb])-Arg(Δ[HbO]) for different age groups in the frontal, left temporal, and right temporal areas. The Arg(Δ[Hb])-Arg(Δ[HbO]) frequency band is 0.01-0.05 Hz. The black line and red line represent the mean and median of the indices, respectively. (d)-(f) Violin plots of the PLI with the age groups in the frontal, left temporal and right temporal areas in 0.01-0.05 Hz.

The results of the two-way ANOVA tests for the PLI measures are shown in Table S16 (see in Supplement Part IV (4)). There are significant interaction effects in all age groups in the frequency band of 0.01-0.1 Hz, 0.05-0.1 Hz, and 0.01-0.1 Hz. This indicates that the PLI was significantly related to the cortical region and age. The main effects of age were significant (p=0.000 for all frequency bands), indicating that the PLI values in different age groups had a significant difference. The statistical tests with Bonferroni correction showed that the spatial differences were not obvious within the groups (Table S17 in Supplement Part IV (4)).

There were significant differences between the children, adult, and healthy elderly age groups for most cortical regions (Tables S18-S20 in Supplement Part IV (4)) for the PLI measurement. For example, the values of children's PLIs in most cortical regions are significantly higher than those of the infant and healthy elderly groups (p<0.01). This finding indicates that PLI is sensitive to brain development. However, it is not sensitive during the first few months of life (i.e. early preterm, term, and 3-4-month-olds infants). This is not the case for phase changes.

The statistical analysis of Arg(Δ[Hb])-Arg(Δ[HbO]) and PLI in group-level that based on the averaged indices of a subject in each cortical region were presented in Supplement Part V.

C. Use of the hemodynamic model for the physiological interpretation of the data

The hemodynamic model assumes a high pass filter relationship between the changes in blood flow velocity and

changes in perfusion pressure according to the known dynamic cerebral autoregulation mechanism. The high pass filter is characterized by a cutoff frequency [2], which is related to the effectiveness of the autoregulation mechanism: the higher the cutoff frequency, the better the functioning autoregulation. We analyzed the changes in Arg(Δ[Hb])-Arg(Δ[HbO]) by increasing the autoregulation cutoff frequency from 0.01 to 0.15 Hz for different capillary ($t^{(c)}$) and venous ($t^{(v)}$) transit times (see Fig. 7). We note that the model predicts a phase lag of Δ[Hb] with respect to Δ[HbO], therefore Arg(Δ[Hb])-Arg(Δ[HbO]) has a negative value. For example, Fig 7(a) shows the Arg(Δ[Hb])-Arg(Δ[HbO]) changes with autoregulation increased from 0.01 to 0.15 Hz. The four curves represent the Arg(Δ[Hb])-Arg(Δ[HbO]) values under the conditions of 1) $t^{(c)}$=0.4 s, $t^{(v)}$=1 s, 2) $t^{(c)}$=1.4 s, $t^{(v)}$=3s, 3) $t^{(c)}$=0.4 s, $t^{(c)}$=3 s, and 4) $t^{(c)}$=1.4 s, $t^{(c)}$=1 s, respectively. As shown in Fig. 7, the Arg(Δ[Hb])-Arg(Δ[HbO]) increases (i.e. becomes less negative) with higher cutoff frequency (i.e. better autoregulation). This is consistent (at least qualitatively) with the experimental data of Fig. 5 and Table II where the phase lag between Δ[Hb] and Δ[HbO] increases from early preterm and term infants (~-240°) to 3-4-month-olds infants and adult (~-195°). This result according to the hemodynamic model can be interpreted as indicative of a developing autoregulation mechanism. It is worth pointing out that Fig. 7 also shows that an increase in blood flow (i.e. a decrease in $t^{(c)}$) would also result in an increase in the relative phase of Δ[Hb] vs. Δ[HbO] oscillations. A similar effect on Arg(Δ[Hb])-Arg(Δ[HbO]) (but not as strong as $t^{(c)}$) is caused by a decrease in $t^{(v)}$, which is also linked to an increase of blood flow.
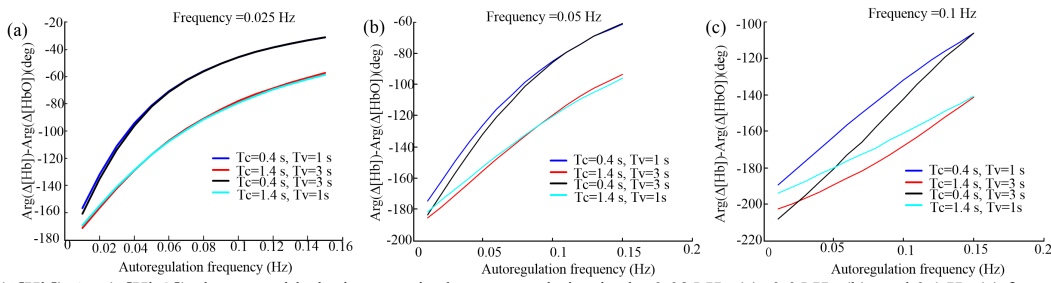
Fig. 7. Arg(Δ[Hb])-Arg(Δ[HbO]) changes with the increase in the autoregulation in the 0.025 Hz (a), 0.05 Hz (b), and 0.1 Hz (c) frequency points.

V. DISCUSSION

Brain structure and functions have been studied extensively using fMRI and fNIRS [32, 33]. However, these studies have been limited to certain age groups. Longitudinal research on brain development over a lifespan is rare [34, 35]. In this study, the influence of the noise on the phase difference was first investigated. Then, we analyzed the phase difference and coupling of Δ[Hb] and Δ[HbO] in age groups from newborn to elderly. The phase difference and PLI measurements were believed to represent the changes in cerebrovascular physiology. To validate it, a hemodynamic model was used to interpret the underlying mechanism associated with the phase difference changes. To our knowledge, this is the first study to investigate phase difference and coupling of Δ[Hb] and Δ[HbO] over such a wide age range. The main findings include: 1) The phase difference progresses to π as the PNA increases in the infant groups (3-7 days to 3-4 months). This anti-phase pattern (i.e. π) persists until late middle age. 2) The coupling of Δ[Hb] and Δ[HbO] (i.e. PLI) also peaks in children and adult age groups. Then, it decreases in the elderly adults. 3) The noise is a non-negligible factor in calculating the phase difference between Δ[Hb] and Δ[HbO]. Overall, significant developmental changes were observed in these fNIRS parameters. The results support the usefulness of hemodynamic imaging biomarkers to monitor brain health across the lifespan.

A. The random noise is a non-negligible factor in calculating the phase difference and coupling strength in fNIRS data analysis

The phase difference and PLI between Δ[Hb] and Δ[HbO] have been developed as important biomarkers to analyze brain development and cognition [12, 15, 16]. To the best of our knowledge, there is no study available that has evaluated the effect of noise on the phase difference between Δ[Hb] and Δ[HbO] being calculated using the modified Beer–Lambert law. In this study, we found that the Δ[HbO] and the Δ[Hb] tend to be anti-phase when the ΔOD is contaminated by random noise. Because of that, we either have to select the signal with high SNR or effectively remove the noise for the phase studies.

B. Tracking brain development using Phase difference

It has been suggested that phase difference is correlated with the cerebrovascular physiology in brain development [11, 36]. For example, Watanabe et al. [12] have suggested a strong correlation between hPod and PNA growth in infants (less than 6-months-old) in the low-frequency band (<0.1 Hz). It has been shown that the hPod progresses to be anti-phase as the PNA increases. Furthermore, there is a significant increase of hPodL

(same as PLI) in the 3-4-month-olds infant group, compared to the neonate group. Consistent with the previous studies, we also found that the Δ[Hb] and Δ[HbO] gradually become anti-phase as the newborns grow.

The spatial- and frequency-specificity (hemodynamic oscillation frequency) of the phase difference was also investigated. Two-way ANOVA and statistical tests confirmed the significant phase differences between the age groups. However, within each age group, there was no obvious spatial specificity. These findings are consistent with those of Taga et al.[7], which compared the hPod of neonates (mean PNA: 4.3 days, range: 2 to 11 days), 3-4-month-olds infants (mean PNA: 111.6 days, range: 102 to 123 days), and 6-month-old infants (mean PNA: 197.0 days, range: 180 to 206 days) channel by channel.

As shown, the phase differences from the 3-4 months to the adults are around π. Based on the previous studies [12, 15], the anti-phase patterns of Δ[Hb] and Δ[HbO] are commonly observed in the age groups over 3-4 months [7]. This may be related to the development of brain circulation, blood flow, metabolic and neurovascular functions [7], and even of the synaptogenesis rates in different brain cortices [37]. We hypothesize that 3-4 months after birth is an important milestone in brain development. In contrast, the phenomenon of wide phase difference distribution in the healthy elderly may be related to the degenerations of cerebrovasculature, neurovascular functions.

C. Sensitivity of the PLIs index to brain development

There was no significant frequency-specificity among the infant age groups (i.e. early preterm, term, and 3-4 months) for the PLI measurement in most of the brain regions. However, there were significant differences among the other age groups (i.e., children, adults, and healthy elderly) in all brain regions. Taga et al.[7] found that the coupling strength (i.e. PLI) of Δ[HbO] and Δ[Hb] increased in the 3-months old infant group compared with the neonate group, over the posterior, but not the anterior, in the frequency band below 0.05 Hz. This study also found that there was no significant PLI increase in frontal or temporal area in the 0.01-0.05 Hz frequency band among the early preterm, term, or 3-4-month-olds infant age groups. Another study [5] analyzed the correlation coefficient between two Δ[HbO] oscillations in the 0.009 Hz to 0.08 Hz frequency band. Notable interhemispheric correlations were observed in the 3- and 6-month-old infant age groups, compared with the neonate group. These studies support that brain development is spatial- and frequency-dependent during the early lifespan. For the wide age distribution of our study, we found that in frontal, left temporal, and right temporal regions, the PLI significantly

decreased with age for the populations over 6-year-old. It suggests that the PLI of the $\Delta[HbO]$ and $\Delta[Hb]$ is a potential parameter for brain development as well as degeneration over the whole lifespan. Moreover, it is known that there is a synaptic refinement and pruning with brain development until mid-adolescence [38, 39]. The excitatory synaptic strength from the prefrontal cortex increases from birth to approximately 5 years old (peak), then decreases and plateaus at about 18 years old [40]. This trajectory is consistent with the changes in PLI. Therefore, our study suggests that the hemodynamic changes during resting state may reflect the typical developmental trajectory associated with synaptic pruning and refinement.

Unlike functional studies, in which transient changes in $\Delta[Hb]$ and $\Delta[HbO]$ (i.e. time series) are crucial, both parameters (i.e. phase changes, coupling strength) used in this study were averaged values obtained from the whole period of resting-state measurements. Therefore, they reflect more on the "status" of the brain [12, 13] than the moment-to-moment changes due to neuronal activation and physiology (i.e. heartbeat).

D. Possible hemodynamic mechanisms of brain development and aging

A previous study [41] has shown that brain development in infants causes the following vascular changes: (1) increased blood volume due to growing capillary density; (2) increased capillary and venous blood flow; and (3) increased mean arterial pressure (limited by cerebral auto-regulation). In addition, regional oxygen consumption increases in healthy infants during their first year [42]. On the contrary, the aging brain includes two distinguishing characteristics: cerebrovascular decline and neuronal degeneration, and they are interrelated [42]. It is known that aging induces hypoperfusion in the brain and blood-brain barrier dysfunction. It has also been found that cerebrovascular aging entails (1) arterial stiffness, (2) endothelial replicative senescence, (3) microvascular rarefaction, (4) narrowing of the vascular lumen, and (5) oxidative stress in inflammation [42]. Lastly, these changes may influence the cerebral autoregulation function. To elucidate the impacts of these underlying changes on the observations of phase differences of $\Delta[HbO]$ and $\Delta[Hb]$ with brain maturation, in this work we used a hemodynamic model [2, 17, 30, 31]. We identified three main physiological parameters that affect the phase lag between $\Delta[Hb]$ and $\Delta[HbO]$: the capillary and venous transit times and the cutoff frequency of the high pass filter which models the dynamic cerebral autoregulation process. The simulations have shown that $Arg(\Delta[Hb])-Arg(\Delta[HbO])$ becomes less negative (i.e. as it happens from preterm to adult) for the following changes: 1) autoregulation process works better (i.e. higher cutoff frequency); 2) the speed of blood flow increases with age (i.e. $t^{(c)}$ and $t^{(v)}$ decrease). There are not many studies in the literature on the dynamic autoregulation in infants, mostly due to the difficulties and risks of inducing controlled variation in blood pressure in such populations. Therefore, some studies have used transcranial Doppler to measure spontaneous changes in blood flow velocity (in main cerebral arteries), following some spontaneous abrupt changes of blood pressure. In the study of Boylan et al. [43], the authors have measured dynamic autoregulation in a cohort of preterm and term babies at risk of neurological injury vs. control groups (all of them undergoing intensive care). They found that in control preterm, dynamic autoregulation was absent, while in control term infants it was intact. This finding is consistent with the results of our model. About the trend of CBF during different life stages, several studies have measured the global or regional CBF from early to young adult age. In one positron emission tomography (PET) study the authors studied regional CBF in a cohort of human subjects from 10 days to 16 years old [44]. In a transcranial Doppler study (TSD) the authors studied the total CBF volume (ml of blood/minute) in a cohort of children from 3 to 18 years old [45]. Both studies came to the same conclusion, that CBF increases from an early age to about 7 years of age, and then it decreases until about 15 years of age where it reaches values typical of adults [45]. The change in CBF is the result of two mechanisms: the increased vascular volume and the increased speed of blood flow. In the two previous studies, these two mechanisms were not disentangled. In another study on infants, the authors monitored a cohort of newborn infants in the first year of age. They measured increases in regional blood volume and flow which was attributed to an increase of capillary density. In another work [46], the authors studied CBF in a cohort of children (7 months - 17 years old) and adults (19-61 years old) by using a functional MRI technique (intracranial 4D flow imaging). The authors were also able to measure the peak velocities in several major arteries of the brain and they found a similar behavior with age as that of CBF of previous studies: an increase of peak velocity until ~7 years of age and a decrease until 18-20 years of age. Typical increase in peak velocity from early age until 7 years old was around 20-25%. By assuming that a similar increase in speed of blood flow occurs also in the microcirculation, we ran our model that (in the frequency range 0.01-0.05 Hz) predicts an average increase in $Arg(\Delta[Hb])-Arg(\Delta[HbO])$ of about 6°. Since the measured increased is around 45° from preterm to three months old, we conclude that the primary effect of these phase change is the development of the dynamic cerebral autoregulation.

E. The merits of parameters and possible application in clinical practice

As we know, the hemodynamic variations of $\Delta[Hb]$ and $\Delta[HbO]$ that derived from fNIRS are the relative changes that arbitrarily assigned zero baselines from the start of the measurement period based on the modified Lambert-Beer law. These raw signals vary between different devices due to the difference of technical principles with different systems. It is almost impossible to evaluable brain development based on the raw fNIRS signals (i.e., $\Delta[Hb]$ and $\Delta[HbO]$). In recent years, some indices, such as functional connection and brain network based on the coupling of $\Delta[HbO]$ (or $\Delta[Hb]$) between different channels, as well as phase difference and the coupling strength between $\Delta[Hb]$ and $\Delta[HbO]$ within the same channel, have been proposed to characterize the brain development and degeneration [5, 16]. All these indices could not be affected by the different optical path lengths of the measurement channels [5].

Compared to the functional connectivity, the phase difference and coupling strength proposed in this study investigated the vascular physiology in the brain. There are

several valuable contributions to our study which will help developing reliable biomarkers in clinical application. Firstly, we quantified the influence of the random noise on the indices of Arg(Δ[Hb])-Arg(Δ[HbO]) and PLI. This paved the way for reliability assessment. Secondly, the ranges of the indices are determined for different age groups. It provides a set of 'standards' for future clinical evaluation. Thirdly, a hemodynamic model was used to interpret the underlying hemodynamic mechanisms of the changes with brain development and aging. Lastly, we have proved that there was no significant difference in the indices of phase difference and PLI collected by the two fNIRS systems from the same person, indicating the robustness of the measurements regardless of the system used.

In relation to neuro cognitive aspect, previous study reported that preterm infants tended to show atypical hemodynamic pattern in response to phonetic processing as characterized by an inverted pattern with decrease of Δ[HbO] and increase of Δ[Hb] [47]. Such differential hemodynamic response to cognitive activity in preterm neonates may relate to immature neurovascular or metabolic system as reflected by differential hPod or PLI in preterm neonates. It is assumed that PLI could work as a biomarker to assess efficient neurocognitive processing and future study should explore this.

In summary, this study paved a way for clinical applications in assessing brain development and aging from infants to the elderly. For instance, phase difference grows from near $\pi/2$ to π during the first 3-4 months of life. The prolonged period of growth might indicate abnormal brain development. Moreover, the π phase difference persists throughout adulthood till the old age in healthy subjects. This can be used to evaluate brain injuries, such as traumatic brain injury, stroke, which might deviate the value. Similar applications can be found for PLI, whose value is significantly higher in children (6-11 years old) compared to other age groups. As the immediate next step, we need to assess the phase difference and PLI in the populations that have brain diseases or developmental challenges.

F. Limitations

There are several limitations to this study that should be mentioned. First, this study used retrospective data from two separate experiments. The probe coverage in infants was different from that of children, adults, and the elderly. However, the spatial specificities of the measurements (Figs. 4, S6, and S7) are not obvious. Thus, the differences in the probes' coverage should have little impact on the results. Second, the age gaps are too wide for the child, adult, and elderly age groups. Mega-analysis will be conducted with more datasets of smaller age gaps in the future. Third, the single-distance NIRS probes used in this study are known to be sensitive to both cerebral and extracerebral hemodynamics. This limitation is less significant in the measurements of infants, but the anatomical differences between infants, children, and adults may themselves introduce age-dependent contributions to our results. However, a NIRS study using multi-distance probes showed that the measurements at a source-detector separation of 3.2 cm (as used in this study) provided the most accurate phase measurements of cerebral hemodynamics [48]. Fourth, we acknowledge that no other physiological signals were measured alongside fNIRS signals. Several studies showed that cerebral and systemic physiological parameters are likely to interfere. The approach of "systemic-physiology augmented functional near-infrared spectroscopy"[49, 50] is helpful to reduce the occurrence of "false positives" in the result [51]. Moreover, further longitudinal studies on the same individual across (periods of) the lifespan should be considered.

VI. CONCLUSION

The trajectories of several imaging parameters have been calculated from newborns to the elderly. These parameters include: 1) the phase difference between Δ[Hb] and Δ[HbO]; 2) the phase coupling index. The distinct age-related changes in these parameters were found. A new hemodynamic model was used to explain these changes with the underlying brain physiologies associated with brain development/aging, like changes in blood flow and cerebral autoregulation mechanism. The model shows that the major effect on the phase is the development of autoregulation. As result, this study demonstrated that these imaging parameters from fNIRS can be used as biomarkers to assess brain health throughout the lifespan.

ACKNOWLEDGMENT

REFERENCES

[1] L. Vasung, E. Abaci Turk, S. L. Ferradal, J. Sutin, J. N. Stout, B. Ahtam, P. Y. Lin, and P. E. Grant, "Exploring early human brain development with structural and physiological neuroimaging," *Neuroimage,* vol. 187, pp. 226-254, Feb 15, 2019.

[2] S. Fantini, "Dynamic model for the tissue concentration and oxygen saturation of hemoglobin in relation to blood volume, flow velocity, and oxygen consumption: Implications for functional neuroimaging and coherent hemodynamics spectroscopy (CHS)," *Neuroimage,* vol. 85 Pt 1, pp. 202-21, Jan 15, 2014.

[3] R. A. Thompson, and C. A. Nelson, "Developmental science and the media. Early brain development," *Am Psychol,* vol. 56, no. 1, pp. 5-15, Jan, 2001.

[4] B. Zhu, E. M. Sevick-Muraca, R. D. Nguyen, and M. N. Shah, "Cap-based Transcranial Optical Tomography in an Awake Infant," *IEEE Transactions on Medical Imaging,* 2020.

[5] F. Homae, H. Watanabe, T. Otobe, T. Nakano, T. Go, Y. Konishi, and G. Taga, "Development of global cortical networks in early infancy," *J Neurosci,* vol. 30, no. 14, pp. 4877-82, Apr 7, 2010.

[6] Y. Yao, W. L. Lu, B. Xu, C. B. Li, C. P. Lin, D. Waxman, and J. F. Feng, "The increase of the functional entropy of the human brain with age," *Sci Rep,* vol. 3, pp. 2853, Oct 9, 2013.

[7] G. Taga, H. Watanabe, and F. Homae, "Spatial variation in the hemoglobin phase of oxygenation and deoxygenation in the developing cortex of infants," *Neurophotonics,* vol. 5, no. 1, pp. 011017, Jan, 2018.

[8] V. Quaresima, S. Bisconti, and M. Ferrari, "A brief review on the use of functional near-infrared spectroscopy (fNIRS) for language imaging studies in human newborns and adults," *Brain Lang,* vol. 121, no. 2, pp. 79-89, May, 2012.

[9] C. Issard, and J. Gervain, "Adult-like processing of time-compressed speech by newborns: A NIRS study," *Dev Cogn Neurosci,* vol. 25, pp. 176-184, Jun, 2017.

[10] R. Hosseini, B. Walsh, F. Tian, and S. Wang, "An fNIRS-based feature learning and classification framework to distinguish hemodynamic

patterns in children who stutter," *IEEE Transactions on Neural Systems and Rehabilitation Engineering,* vol. 26, no. 6, pp. 1254-1263, 2018.

[11] M. L. Pierro, A. Sassaroli, P. R. Bergethon, B. L. Ehrenberg, and S. Fantini, "Phase-amplitude investigation of spontaneous low-frequency oscillations of cerebral hemodynamics with near-infrared spectroscopy: a sleep study in human subjects," *Neuroimage,* vol. 63, no. 3, pp. 1571-84, Nov 15, 2012.

[12] H. Watanabe, Y. Shitara, Y. Aoki, T. Inoue, S. Tsuchida, N. Takahashi, and G. Taga, "Hemoglobin phase of oxygenation and deoxygenation in early brain development measured using fNIRS," *Proc Natl Acad Sci U S A,* vol. 114, no. 9, pp. E1737-E1744, Feb 28, 2017.

[13] Z. Liang, Y. Minagawa, H. C. Yang, H. Tian, L. Cheng, T. Arimitsu, T. Takahashi, and Y. Tong, "Symbolic time series analysis of fNIRS signals in brain development assessment," *J Neural Eng,* vol. 15, no. 6, pp. 066013, Dec, 2018.

[14] L. Cai, Q. Dong, and H. Niu, "The development of functional network organization in early childhood and early adolescence: A resting-state fNIRS study," *Dev Cogn Neurosci,* vol. 30, pp. 223-235, Apr, 2018.

[15] C. Issard, and J. Gervain, "Variability of the hemodynamic response in infants: Influence of experimental design and stimulus complexity," *Dev Cogn Neurosci,* vol. 33, pp. 182-193, Oct, 2018.

[16] G. Taga, H. Watanabe, and F. Homae, "Developmental changes in cortical sensory processing during wakefulness and sleep," *Neuroimage,* vol. 178, pp. 519-530, Sep, 2018.

[17] J. M. Kainerstorfer, A. Sassaroli, and S. Fantini, "Coherent hemodynamics spectroscopy in a single step," *Biomed Opt Express,* vol. 5, no. 10, pp. 3403-16, Oct 1, 2014.

[18] A. A. o. Pediatrics, A. C. o. Obstetricians, Gynecologists, and C. o. O. Practice, "The Apgar Score," *Pediatrics,* vol. 117, no. 4, pp. 1444-1447, 2006.

[19] V. Jurcak, D. Tsuzuki, and I. Dan, "10/20, 10/10, and 10/5 systems revisited: their validity as relative head-surface-based positioning systems," *Neuroimage,* vol. 34, no. 4, pp. 1600-11, Feb 15, 2007.

[20] M. Cope, and D. T. Delpy, "System for long-term measurement of cerebral blood and tissue oxygenation on newborn infants by near infra-red transillumination," *Med Biol Eng Comput,* vol. 26, no. 3, pp. 289-94, May, 1988.

[21] L. Cai, Q. Dong, M. Wang, and H. Niu, "Functional near-infrared spectroscopy evidence for the development of topological asymmetry between hemispheric brain networks from childhood to adulthood," *Neurophotonics,* vol. 6, no. 2, pp. 025005, Apr, 2019.

[22] H. Niu, Z. Zhu, M. Wang, X. Li, Z. Yuan, Y. Sun, and Y. Han, "Abnormal dynamic functional connectivity and brain states in Alzheimer's diseases: functional near-infrared spectroscopy study," *Neurophotonics,* vol. 6, no. 2, pp. 025010, Apr, 2019.

[23] N. Kollias, and W. B. Gratzer, "Tabulated molar extinction coefficient for hemoglobin in water," Wellman Laboratories, Harvard Medical School, Boston 5, 150–161 (1999).

[24] Y. Zhao, L. Qiu, Y. Sun, C. Huang, and T. Li, "Optimal hemoglobin extinction coefficient data set for near-infrared spectroscopy," *Biomedical Optics Express,* vol. 8, no. 11, pp. 5151-5159, 2017.

[25] M. Cope, D. T. Delpy, E. O. Reynolds, S. Wray, J. Wyatt, and P. van der Zee, "Methods of quantitating cerebral near infrared spectroscopy data," *Adv Exp Med Biol,* vol. 222, pp. 183-9, 1988.

[26] G. Strangman, M. A. Franceschini, and D. A. Boas, "Factors affecting the accuracy of near-infrared spectroscopy concentration calculations for focal changes in oxygenation parameters," *Neuroimage,* vol. 18, no. 4, pp. 865-79, Apr, 2003.

[27] A. M. Chiarelli, E. L. Maclin, M. Fabiani, and G. Gratton, "A kurtosis-based wavelet algorithm for motion artifact correction of fNIRS data," *Neuroimage,* vol. 112, pp. 128-137, May 15, 2015.

[28] P. Pinti, D. Cardone, and A. Merla, "Simultaneous fNIRS and thermal infrared imaging during cognitive task reveal autonomic correlates of prefrontal cortex activity," *Sci Rep,* vol. 5, pp. 17471, Dec 3, 2015.

[29] P. Berens, "CirkStat: AMatlab Toolbox for Circular Statistics," *Journal of Statistical Software,* vol. 31, pp. 1-21, 2009.

[30] J. M. Kainerstorfer, A. Sassaroli, B. Hallacoglu, M. L. Pierro, and S. Fantini, "Practical steps for applying a new dynamic model to near-infrared spectroscopy measurements of hemodynamic oscillations and transient changes: implications for cerebrovascular and functional brain studies," *Acad Radiol,* vol. 21, no. 2, pp. 185-96, Feb, 2014.

[31] S. Fantini, "A haemodynamic model for the physiological interpretation of in vivo measurements of the concentration and oxygen saturation of haemoglobin," *Phys Med Biol,* vol. 47, no. 18, pp. N249-57, Sep 21, 2002.

[32] M. Abtahi, S. B. Borgheai, R. Jafari, N. Constant, R. Diouf, Y. Shahriari, and K. Mankodiya, "Merging fNIRS-EEG Brain Monitoring and Body Motion Capture to Distinguish Parkinson's Disease," *IEEE Transactions on Neural Systems and Rehabilitation Engineering,* 2020.

[33] L. Xiao, A. Zhang, B. Cai, J. M. Stephen, T. W. Wilson, V. D. Calhoun, and Y.-P. Wang, "Correlation Guided Graph Learning to Estimate Functional Connectivity Patterns from fMRI Data," *IEEE Transactions on Biomedical Engineering,* 2020.

[34] X. N. Zuo, C. Kelly, A. Di Martino, M. Mennes, D. S. Margulies, S. Bangaru, R. Grzadzinski, A. C. Evans, Y. F. Zang, F. X. Castellanos, and M. P. Milham, "Growing together and growing apart: regional and sex differences in the lifespan developmental trajectories of functional homotopy," *J Neurosci,* vol. 30, no. 45, pp. 15034-43, Nov 10, 2010.

[35] R. F. Betzel, L. Byrge, Y. He, J. Goni, X. N. Zuo, and O. Sporns, "Changes in structural and functional connectivity among resting-state networks across the human lifespan," *Neuroimage,* vol. 102 Pt 2, pp. 345-57, Nov 15, 2014.

[36] G. Taga, Y. Konishi, A. Maki, T. Tachibana, M. Fujiwara, and H. Koizumi, "Spontaneous oscillation of oxy- and deoxy- hemoglobin changes with a phase difference throughout the occipital cortex of newborn infants observed using non-invasive optical topography," *Neurosci Lett,* vol. 282, no. 1-2, pp. 101-4, Mar 17, 2000.

[37] L. Cornelissen, S. E. Kim, J. M. Lee, E. N. Brown, P. L. Purdon, and C. B. Berde, "Electroencephalographic markers of brain development during sevoflurane anaesthesia in children up to 3 years old," *Br J Anaesth,* vol. 120, no. 6, pp. 1274-1286, Jun, 2018.

[38] P. R. Huttenlocher, "Synaptic density in human frontal cortex - developmental changes and effects of aging," *Brain Res,* vol. 163, no. 2, pp. 195-205, Mar 16, 1979.

[39] L. A. Glantz, J. H. Gilmore, R. M. Hamer, J. A. Lieberman, and L. F. Jarskog, "Synaptophysin and postsynaptic density protein 95 in the human prefrontal cortex from mid-gestation into early adulthood," *Neuroscience,* vol. 149, no. 3, pp. 582-91, Nov 9, 2007.

[40] T. R. Insel, "Rethinking schizophrenia," *Nature,* vol. 468, no. 7321, pp. 187-93, Nov 11, 2010.

[41] G. Greisen, "Autoregulation of cerebral blood flow in newborn babies," *Early Hum Dev,* vol. 81, no. 5, pp. 423-8, May, 2005.

[42] M. A. Franceschini, S. Thaker, G. Themelis, K. K. Krishnamoorthy, H. Bortfeld, S. G. Diamond, D. A. Boas, K. Arvin, and P. E. Grant, "Assessment of infant brain development with frequency-domain near-infrared spectroscopy," *Pediatr Res,* vol. 61, no. 5 Pt 1, pp. 546-51, May, 2007.

[43] G. B. Boylan, K. Young, R. B. Panerai, J. M. Rennie, and D. H. Evans, "Dynamic cerebral autoregulation in sick newborn infants," *Pediatr Res,* vol. 48, no. 1, pp. 12-7, Jul, 2000.

[44] T. Takahashi, R. Shirane, S. Sato, and T. Yoshimoto, "Developmental changes of cerebral blood flow and oxygen metabolism in children," *AJNR Am J Neuroradiol,* vol. 20, no. 5, pp. 917-22, May, 1999.

[45] M. Schoning, and B. Hartig, "Age dependence of total cerebral blood flow volume from childhood to adulthood," *J Cereb Blood Flow Metab,* vol. 16, no. 5, pp. 827-33, Sep, 1996.

[46] C. Wu, A. R. Honarmand, S. Schnell, R. Kuhn, S. E. Schoeneman, S. A. Ansari, J. Carr, M. Markl, and A. Shaibani, "Age-Related Changes of Normal Cerebral and Cardiac Blood Flow in Children and Adults Aged 7 Months to 61 Years," *J Am Heart Assoc,* vol. 5, no. 1, Jan 4, 2016.

[47] T. Arimitsu, Y. Minagawa, T. Yagihashi, M. O. Uchida, A. Matsuzaki, K. Ikeda, and T. Takahashi, "The cerebral hemodynamic response to phonetic changes of speech in preterm and term infants: The impact of postmenstrual age," *NeuroImage: Clinical,* vol. 19, pp. 599-606, 2018.

[48] G. Blaney, A. Sassaroli, T. Pham, N. Krishnamurthy, and S. Fantini, "Multi-Distance Frequency-Domain Optical Measurements of Coherent Cerebral Hemodynamics," *Photonics,* vol. 6, no. 3, pp. 83, 2019.

[49] F. Scholkmann, T. Hafner, A. J. Metz, M. Wolf, and U. Wolf, "Effect of short-term colored-light exposure on cerebral hemodynamics and oxygenation, and systemic physiological activity," *Neurophotonics,* vol. 4, no. 4, pp. 045005, Oct, 2017.

[50] A. J. Metz, S. D. Klein, F. Scholkmann, and U. Wolf, "Continuous coloured light altered human brain haemodynamics and oxygenation assessed by systemic physiology augmented functional near-infrared spectroscopy," *Sci Rep,* vol. 7, no. 1, pp. 10027, Aug 30, 2017.

[51] I. Tachtsidis, and F. Scholkmann, "False positives and false negatives in functional near-infrared spectroscopy: issues, challenges, and the way forward," *Neurophotonics,* vol. 3, no. 3, pp. 031405, Jul, 2016.